Journal of Advanced Scientific Research

Available online through http://www.sciensage.info

ISSN 0976-9595

Research Article

CORROSION PROTECTIVE BEHAVIOR OF MoO_3 AND Y_2O_3 COATED AZ31 ALLOY

L. Sutha[1,2], A. Cyril*[2]

[1]Research Scholar, Department of Industrial Chemistry, Alagappa University, Karaikudi, India

[2]Post graduate &Research Department of Chemistry, Raja Dorasingam Government Arts College, Sivaganga, Tamilnadu, India

*Corresponding author: cyrilchemistry@gmail.com

ABSTRACT

Herein, we have reported formulation of MoO_3 and Y_2O_3 coatings over AZ31 alloy using organic binder. The coatings were characterized using X-ray diffraction (XRD), Fourier Transform Infrared Spectroscopy (FTIR), Raman spectroscopy and Field Emission Scanning Electron Microscope (FESEM). The results indicate that the powders exhibit high crystalline nature. The electrochemical polarization studies were conducted using three electrode systems in 3.5% NaCl electrolyte. The corrosion resistance was examined using electrochemical impedance spectroscopy technique. The uncoated AZ31 alloy exhibited the corrosion potential (E_{corr}) of -1.7 V (SCE) and corrosion current density of 3.4 x 10^{-4} mA/cm^2. Similarly, the MoO_3 coated AZ31 alloy showed the corrosion potential (E_{corr}) of -1.5 V (SCE) and corrosion current density of 3.73 x 10^{-10} mA/cm^2. Further, the Y_2O_3 coated AZ31 alloy showed the E_{corr} of -1.3 V (SCE) and corrosion current density of 1.28 x 10^{-10} mA/cm^2. Similarly, the impedance analysis also provides strong evidence that the Y_2O_3 coated AZ31 alloy exhibited higher corrosion resistance among all the samples. From the results, it is evident that the Y_2O_3 coated AZ31 alloy showed enhanced corrosion protection properties.

Keywords: Corrosion, MoO_3 coating, Y_2O_3 coating, Mg alloy, AZ31.

1. INTRODUCTION

Magnesium and its alloys demonstrated excellent performance in aerospace applications due to their low density and high strength. Nevertheless, magnesium and its alloys suffer high corrosion due to more negative electromotive force and hence, they undergo corrosion in aqueous mediums [1-4]. In this view, the research has been focused on the enhancement of corrosion resistance [5-12]. Many attempts have been directed on the development of surface coatings, where the application of coatings has demonstrated as an excellent method to improve the corrosion resistance of magnesium and its alloys [13-15]. However, still much scope is yet to be done in the direction to improve the corrosion resistance of magnesium alloys. The surface and interconnected porosity play a vital role in determining the corrosion rate of inorganic coating and it is evident that the porosity of the coatings should be low to achieve higher corrosion protection.

Herein, we have formulated MoO_3 and Y_2O_3 coatings over AZ31 alloy using organic binder. The organic binder provided porous (inter connected) free coatings. The electrochemical polarization studies were conducted in 3.5% NaCl electrolyte using three electrode systems, where platinum foil as counter, saturated calomel electrode (SCE) as reference and AZ31 alloy (with and without coatings) employed as working electrode. The uncoated AZ31 alloy exhibited the corrosion potential (E_{corr}) of -1.7 V (SCE) and corrosion current density of 3.4 x 10^{-4} mA/cm^2. Similarly, the MoO_3 coated AZ31 alloy showed the corrosion potential (E_{corr}) of -1.5 V (SCE) and corrosion current density of 3.73 x 10^{-10} mA/cm^2. The Y_2O_3 coated AZ31 alloy showed the corrosion potential (E_{corr}) of -1.3 V (SCE) and corrosion current density of 1.28 x 10^{-10} mA/cm^2. This work paves new pathways to improve corrosion resistance of AZ31 alloy.

2. MATERIAL AND METHODS

2.1. Chemicals

Yttrium(III) nitrate hexahydrate ($Y(NO_3)_3{\cdot}6H_2O$, 99.8%, CAS No: 13494-98-9), Ammonium hepta-molybdate ($(NH_4)_6Mo_7O_{24}$), Sodium hydroxide (NaOH, CAS No: 1310-73-2), Poly(ethylene glycol) (PEG_3, Bioultra 8000, CAS No: 25322-68-3) and Nitric acid were purchased from Sigma Aldrich.

2.2. Synthesis of MoO_3

The MoO_3 nano-particles were synthesized by hydrothermal route. In brief, 1mM of Ammonium heptamolybdate ($(NH_4)_6Mo_7O_{24}$) was dissolved on distilled water under stirring, to this, nitric acid (2M) was added drop wise and the resultant solution was transferred to hydrothermal Teflon lined autoclave and kept in furnace at 180°C for the period of 10 h. The resulted solution was centrifuged and dried for characterization.

2.3. Synthesis of Y_2O_3

The Y_2O_3 nano-particles were synthesized by hydro-thermal route. In brief, 1mM of Yttrium(III) nitrate hexahydrate was dissolved on distilled water under stirring, to this, NaOH solution (pH=~12) was added drop wise and the resultant solution with precipitation was transferred to hydrothermal Teflon lined autoclave and kept in furnace at 180°C for the period of 10 h. The resulted solution was centrifuged and dried for characterization.

2.4. Sample preparation

The electrochemical polarization study samples were fabricated with the following procedure. First, the small samples were cut into 12 x 12 x 5 mm in size using wire EDM. Before the development of coatings over alloy samples, the samples were undergone metallurgical polishing using SiC grit emery papers, from 200 to 1200 grit papers, and finally 0.5 microns cloth polishing. Further, the samples were washed and dried at room temperature.

First, PEG was dissolved in anhydrous ethanol for 10 min at 50°C and mixed with synthesized MoO_3 and Y_2O_3 (separately) powders till homogenous mixture and kept in oven for 12 h and the resultant was applied on AZ31 alloy using doctor blade method

2.5. Electrochemical experiments

The electrochemical polarization of uncoated AZ31 alloy, MoO_3 and Y_2O_3 coated AZ31 alloy was explored in 3.5% NaCl electrolyte using three electrodes system, where Pt foil as counter electrode, SCE (saturated calomel electrode) and Mg alloys as working electrode. Electrochemical impedance was also carried out on the all the samples using the same system.

3. RESULTS AND DISCUSSION

3.1. X-ray diffraction analysis:

The crystalline nature of uncoated AZ31, MoO_3 coated AZ31 and Y_2O_3 coated AZ31 alloy was analyzed by X-ray diffraction analysis and presented in figs. 1-3.

The bare or uncoated AZ31 alloy demonstrated the high crystalline peaks, which were well matched to the standard JCPDS file no 35-0821, exhibiting hexagonal crystal structure for Mg alloy (a=b=3.2094 Å and c=5.211Å) and belongs to P63/mmc space group. This analysis is also well matched with reported literature [16-19].

The MoO_3 coated AZ31 alloy XRD pattern is shown in fig. 2. The Molybdenum oxide peaks well matched with standard JCPDS file no: 05-0508. The pattern exhibit the planes of (020), (110), (040), (021) indicate orthorhombic α-MoO_3 structure (a=3.9620 b=13.858 c=3.6970 Å) that belongs to Pbnm space group. The plane (060) indicates anisotropic growth at corner sharing chains of MoO_6 octahedra with two similar chains and forms stoichiometric layers in *ac*-plane of MoO_3 [20-24].

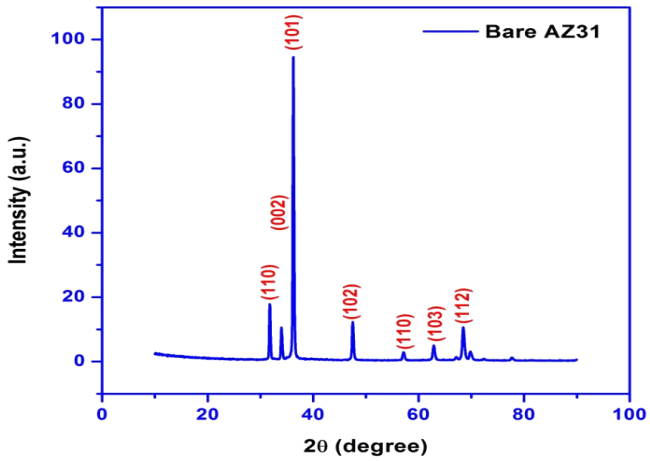

Fig. 1: XRD pattern of AZ31 alloy

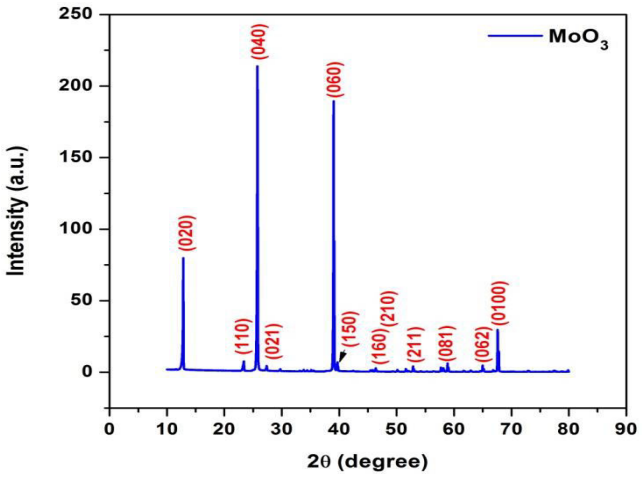

Fig. 2: XRD pattern for MoO_3 coated AZ31 alloy

Further, the Y_2O_3 coated AZ31 alloy XRD pattern is shown in fig. 3. The diffraction peaks centered at 20.65° (211), 29.30° (222), 33.89° (400), 36.15° (411) 39.89° (332), 43.59° (134), 48.692° (440), 53. 48° (611), 56.40° (541), 57.90° (622), 59.35° (136), 60.80° (444), 64.80° (127), 71.40° (800), and 72.65° (811), which are matched well with the standard body-centered cubic Y_2O_3 (JCPDS card no.88-1040) [25-27].

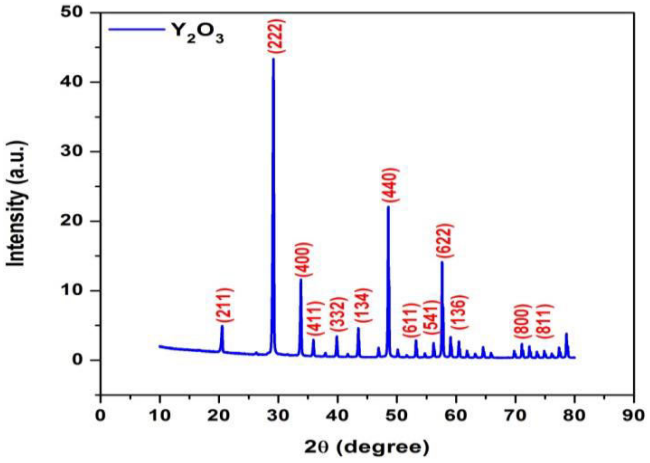

Fig. 3: XRD pattern for Y_2O_3 coated AZ31 alloy

3.2. FESEM analysis

The surface morphology of MoO_3 and Y_2O_3 coatings are presented in figs. 4 and 5, respectively. Both the oxide powders show their individual particles with irregular shapes or morphology. Some spherical and individual particles are noticed in the both the images, which are corresponds to the respective oxide particles.

3.3. FTIR analysis

The Fourier Transform Infrared Spectroscopy (FTIR) analysis of MoO_3 and Y_2O_3 were carried out and presented in fig. 6 and 7, respectively.

Figure 6 shows the FTIR spectrum of MoO_3 compound. The peak at 493 cm^{-1} is due to the stretching mode of Mo-O terminal, while 866 cm^{-1} is attributed to the bending vibration mode of Mo-O-Mo. The peak at 1522 cm^{-1} is attained due to the C=O stretching and 3688 cm^{-1} is due to the hydroxyl groups in the compound [28-31].

Similarly, fig.7 shows the FTIR spectrum of Y_2O_3 compound, where it is noticed that the peaks at 450, 570, 1577, 3040 and 3680 cm^{-1}. The bands at 450, 570 cm^{-1} can be distinguished and corresponds to vibration Y-O bands in the yttria structure [32-34]. The band at 3040 and 3680 cm^{-1} are attributed to olefinic and hydroxyl stretching.

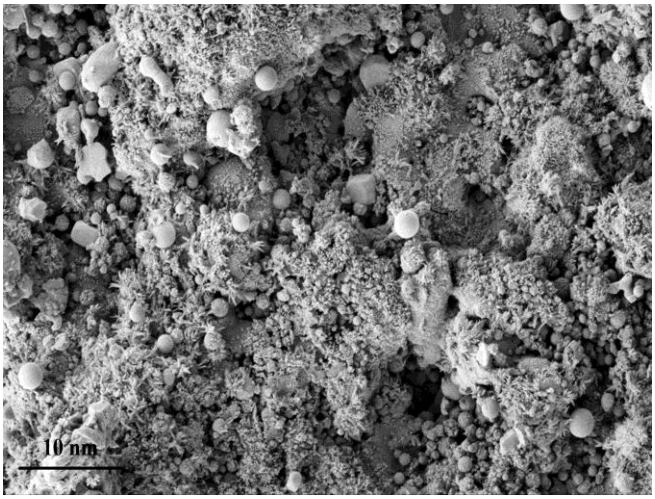

Fig. 4: Surface morphology of MoO_3 coated AZ31 alloy

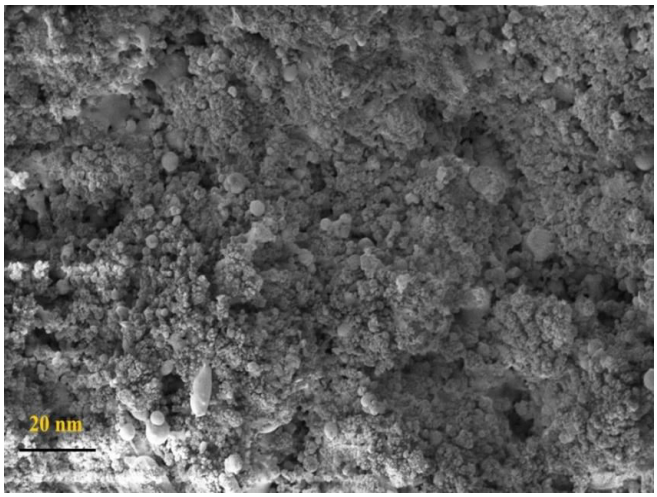

Fig. 5: Surface morphology of Y_2O_3 coated AZ31 alloy

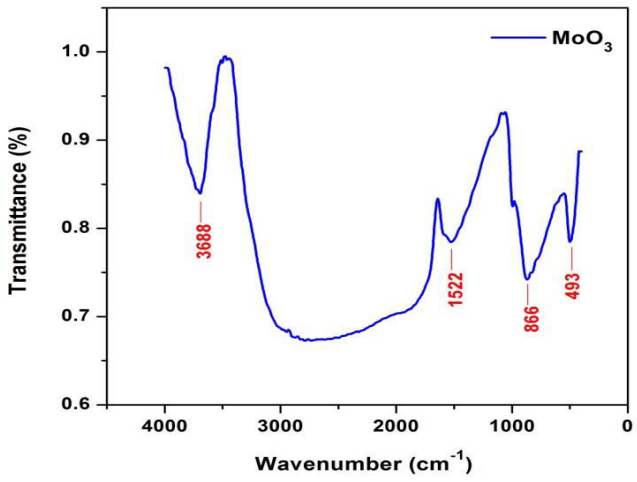

Fig. 6: FTIR spectrum of MoO_3 compound

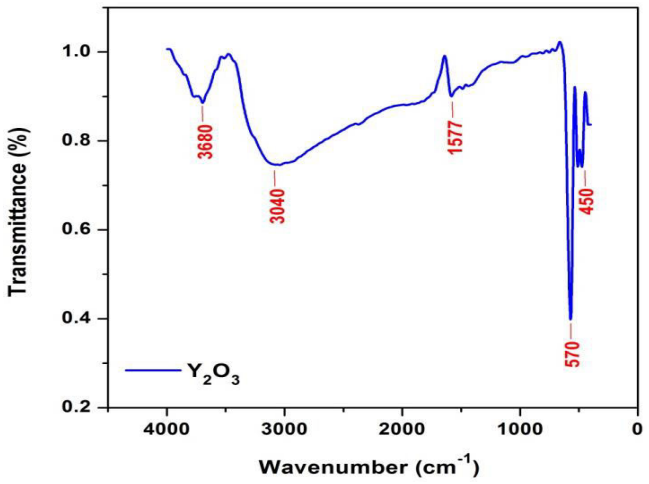

Fig. 7: FTIR spectrum of Y_2O_3 compound

3.4. Raman analysis

The Raman spectrum of MoO_3 compound is presented in fig. 8. The Raman modes were observed at 115, 160, 285, 335, 375, 470, 666, 820 and 996 cm^{-1}. The peak at 375 cm^{-1} is attributed to the scissoring of O-Mo-O. The band at 335 cm^{-1} can be assign to O-Mo-O bending, and 285 cm^{-1} can be assign to O=Mo=O wagging. Further, the peaks at 666 cm^{-1} are attributed to O-Mo-O stretching; the 822 cm^{-1} and 996 cm^{-1} peaks are corresponds to the stretching of terminal Mo=O bonds [35-38].

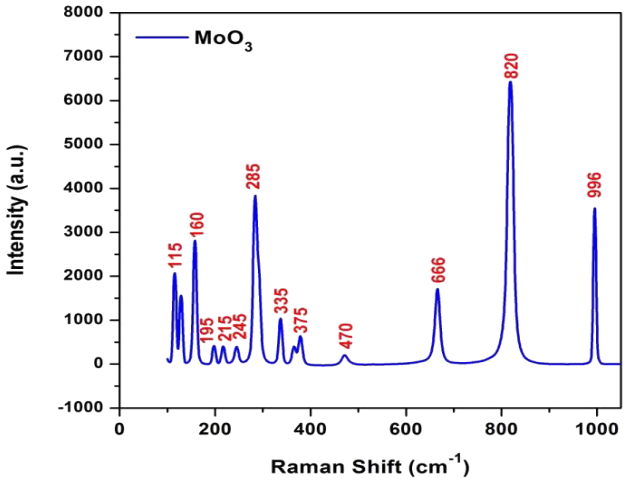

Fig. 8: Raman spectrum of MoO_3 compound

The Raman spectrum of Y_2O_3 compound is presented in fig. 9. The Raman modes were observed at 122, 165, 211, 262, 328, 443, 515, 591, 881 and 971 cm^{-1}. The most intense band at 375 cm^{-1} demonstrates the large polarizability vibration and it is characteristic peak of cubic yttria. While the rest of peaks represent A_g, E_g, and F_g and F_u are Raman active of yttria cubic strictures [39, 40].

Moreover, the disorder-induced peak (1350 cm^{-1}) and graphite peak (1580cm^{-1}), which are caused by C when TaC + C phase is formed.

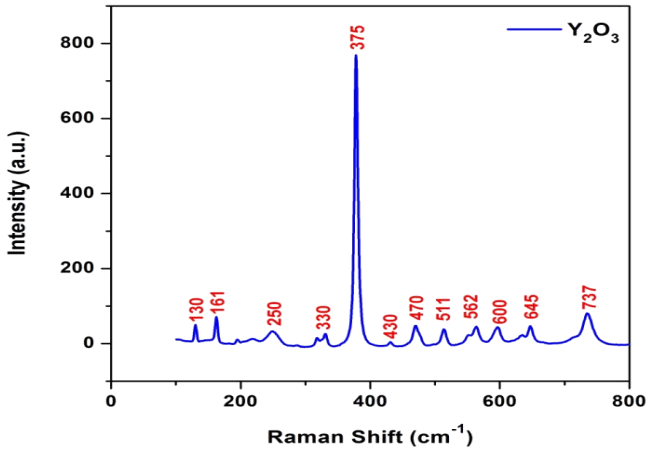

Fig. 9: Raman spectrum of Y_2O_3 compound

3.5. Electrochemical analysis

Electrochemical polarization studies of uncoated AZ31 alloy, MoO_3 and Y_2O_3 coatings are presented in figs. 10-12. The electrochemical studies were carried out in 3.5% NaCl electrolyte using three electrode assembly cell systems. As described in experimental procedure, pt foil was used as counter electrode, SCE as reference electrode and coated and uncoated AZ31 alloy as working electrodes.

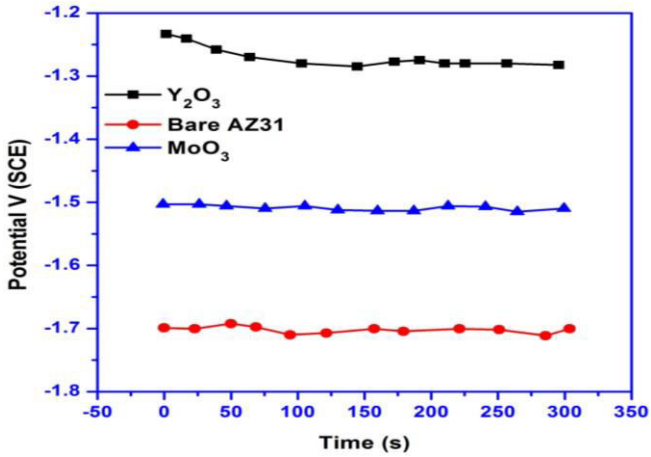

Fig. 10: Open circuit potentials of bare AZ31 and Y_2O_3 coated and MoO_3 coated AZ31 alloy

The open circuit potentials are considered corrosion potentials for all the electrodes and the recorded results

are shown in fig. 10. From the figure, it is noticed that the uncoated sample exhibited corrosion potential of 1.7 V (SCE), while MoO_3 coated AZ31 alloy demonstrated corrosion potential of 1.5 V (SCE) and Y_2O_3 coated alloy showed 1.3 V (SCE) as corrosion potential. In comparison, the Y_2O_3 coated AZ31 alloy exhibited more noble shift in open circuit potential than that of others.

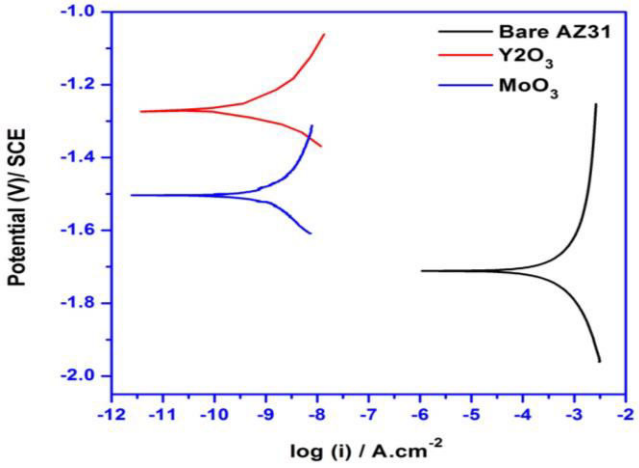

Fig. 11: Tafel plots of bare AZ31 and Y_2O_3 coated and MoO_3 coated AZ31 alloy

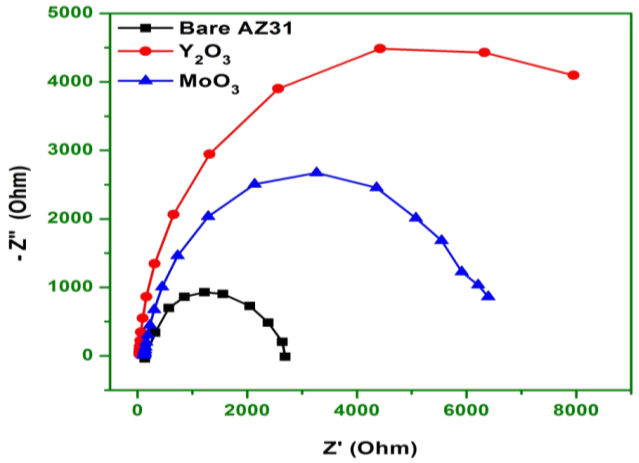

Fig. 12: Electrochemical impedance curves of bare AZ31 and Y_2O_3 coated AZ31 alloy and MoO_3 coated AZ31 alloy

The Tafel plots of uncoated AZ31 alloy and Y_2O_3 coated and MoO_3 coated AZ31 alloy are shown in fig. 11. The calculated corrosion rate are as follows, the uncoated AZ31 alloy exhibited 3.4 x 10^{-4} mA/cm^2. Further, the MoO_3 coated AZ31 alloy showed the corrosion current density of 3.73 x 10^{-10} mA/cm^2 and in addition to this, the Y_2O_3 coated AZ31 alloy showed the corrosion current density of 1.28 x 10^{-10} mA/cm^2. The EIS images Fig. 12, shows that uncoated AZ31 alloy demonstrated less corrosion resistance, and the Y_2O_3 coated AZ31 alloy showed excellent resistance, while MoO_3 coated AZ31 alloy demonstrated intermediate performance.

White et al fabricated TiO_2 coating over AZ31 alloy using plasma electrolytic oxidation (PEO), where the coating demonstrated enhanced corrosion protection to Mg alloy [41]. The coating showed the noble shift in corrosion potential upto -1.4 V (SCE) in 3.5% NaCl electrolyte. Similarly, Chen et al developed MgO, $MgAl_2O_4$ and $MgSiO_3$ composed coating through microarc oxidation process and demonstrated that the ceramic coated sample showed corrosion potential of ~1.5 V in 3.5% NaCl medium [42]. Tan et al developed Ca-P coatings on AZ31 Mg alloy via chemical deposition and noticed that Ca-P coating dramatically decreased the corrosion rates and improved corrosion resistance. The authors demonstrated the corrosion potential up to -1.5 V (SCE) in 3.5% NaCl medium [43]. In this work, the Y_2O_3 coated AZ31 alloy showed the corrosion potential of ~ -1.3 V (SCE) and corrosion current density of 1.28 x 10^{-10} mA/cm^2 in 3.5% NaCl medium. This work demonstrated enhanced corrosion protection for AZ31 alloy with proposed coatings in comparison with literature and paves new pathway for the corrosion protection improvement of magnesium alloys.

4. CONCLUSION

The MoO_3 (molybdenum oxide) and Y_2O_3 (yttrium oxide) coating was developed on AZ31 alloy using polymer binder. The uncoated AZ31 alloy exhibited corrosion current density of 3.4 x 10^{-4} mA/cm^2. The MoO_3 coated AZ31 alloy showed the corrosion current density of 3.73 x 10^{-10} mA/cm^2 and the Y_2O_3 coated AZ31 alloy showed the corrosion current density of 1.28 x 10^{-10} mA/cm^2. The EIS results also reveal the same trend and the Y_2O_3 coated AZ31 alloy demonstrated higher corrosion resistance than of bare and MoO_3 coated AZ31 alloy and bare AZ31 alloy

Conflict of interest

Authors declared that there is no conflict of interest

5. REFERENCES

1. Mordike BL, Ebert T. *Mater. Sci.Eng*, 2001; **302:**37-45.
2. Wu RZ, Yan YD, Wang GX, Murr LE, Han W,

Zhang ZW, Zhang ML. *Int. Mater. Rev.*, 2015; **60:**65-100.
3. Hou L, Wang T, Wu R, Zhang J, Zhang M, Dong A, Sun B, Betsofen S, Krit B. *J. Mater. Sci. Technol.*, 2018; **34:**317-323.
4. Thomas S, Medhekar NV, Frankel GS, Birbilis N. *Curr. Opin. Solid State Mater. Sci.*, 2015; **19:**85-94.
5. Danaie M, Asmussen RM, Jakupi P, Shoesmith D W, Bottona GA. *Corros. Sci.*, 2013; **77:**151-163.
6. Shahabi-Navid M, Esmaily M, Svensson JE, Halvarsson M, Nyborg L, Cao Y, Johansson LG. *J. Electrochem. Soc.*, 2014; **61:**C277-C287.
7. Esmaily M, Blücher D B, Lindstrom R W, Svensson JE, Johansson LG. *J. Electrochem. Soc.*, 2015; **162:**C260-C269
8. Ha H, Kim H, Baek S, Kim B, Sohn S, Shin H, et al. Lee J G, Park SS. *Scr. Mater.*, 2015; **109:**38-43.
9. Pu Z, Yang S, Song G.-L, Dillon Jr. O W, Puleo D A, Jawahir IS. *Scr. Mater.*, 2011; **65:**520-523.
10. Asmussen RM, Jakupi P, Danaie M, Bottonb GA, Shoesmith DW. *Corros. Sci.*, 2013; **75:**114-122.
11. Esmaily M, Shahabi-Navid M, Svensson JE, Halvarsson M, Nyborg L, Cao Y, et al. *Corros. Sci.*, 2015; **90:**420-433.
12. Singh Raman RK, Birbilis N, Efthimiadis J. *Corros. Eng. Sci. Technol.*, 2004; **39:**346-350.
13. Han B. Int. *J. Electrochem. Sci.*, 2017; 9829-9843.
14. Wu G, Dai W, Zheng H, Wang A. *Surf. Coat. Technol.*, 2010; **205:** 2067-0073.
15. Yaowei Y, Wei F, Xiang Z, Qilin D, Jianguo Y. *Rare Metal Mat Eng*, 2017; **46:**3176-3181.
16. Sunil BR, Ganesh KV, Pavan P, Vadapalli G, Swarnalatha C, Swapna P, et al. *J. Magnes. Alloy*, 2016; **4:**15-21.
17. Fridrich HE, Mordike BL. *Magnesium Technology*, Springer, Germany, 2006.
18. Mordike BL, Ebert T. *Mater. Sci. Eng. A.*, 2001; **302:**37-45.
19. Avedesian MM, Baker H. ASM Specialty Handbook, Magnesium and Magnesium Alloys, ASM International, USA, 1999.
20. Zhou J, Song J, Li H, Feng X, Huang Z, Chen S, et al. *New J. Chem.*, 2015; **39:**8780-8786.
21. Sun Y, Wang J, Zhao B, Cai R, Ran R, Shao Z. *J. Mater. Chem. A*, 2013; **1:**4736-4746.
22. Prakash NG, Dhananjaya M, Narayana AL, Maseed H, Srikanth VVSS, Hussain OM. *Appl. Phys. A.*, 2019; 125(8).
23. Zhou J, Deng SZ, Xu NS, Chen J, She JC. *Appl. Phys. Lett.,* 2003; **83:**2653-2655.
24. Reddya Subba Ch V, Walker EH, Chen W, Mho S. *J. Power Sources,* 2008; **183:**330-333.
25. Wang H, Qian C, Yi Z, Rao L, Liu H, Zeng S. *Advances in Condensed Matter Physics,* 2013; 1-6.
26. Jayasankar K, Pandey A, Mishra BK, Das S. *Mater. Chem. Phys.*, 2016; **171:**195-200.
27. Tamrakar RK, Upadhyay K, Bisen DP. *J Radiat Res Appl Sc.*, 2014; **7:**526-531.
28. Kothaplamoottil Sivan S, Padinjareveetil AKK, Padil VVT, Pilankatta R, George B, Senan C, Varma R. S. *Clean Technol Environ Policy*, 2019.
29. Guzman G, Yebka B, Livage J, Julien C. *Solid State Ion*, 1996; **86:**407-413.
30. Xia T, Li Q, Liu X, Meng J, Cao X, *J Phys Chem B.*, 2006; **110:**2006-2012.
31. Sanchez C, Nigen M, Mejia Tamayo V, Doco T, Williams P, Amine C. *Food Hydrocoll*, 2018; **78:**140-160.
32. Kruk A, Wajler A, Bobruk M, Adamczyk A, Mrózek M, Gawlik W, et al. *J Eur Ceram Soc.*, 2017; **37:**4129-4140.
33. Vishnuvardhan T K, Kulkarni V R, Basavaraja C, Raghavendra S C, *B Mater. Sci.*, 2006; **29:** 77-83.
34. da Villa L D, Stucchi E B, Davalos M R. *J. Mater. Chem.*, 1997; **10:** 2113-2116.
35. Patel S, Dewangan K, Srivastav S, Verma N, Jena, Singh P, Kumar A et al. *Advanced Materials Letters*, 2018; 9.
36. Guan X, Ren Y, Chen S. *J Mater Sci.*, 2020; **55:**5808-5822.
37. Yang XF, Ding HY, Zhang D. *Cryst Res Technol.*, 2011; **46:**1195-1201
38. Bhattacharya S, Dinda D, Saha SK. *J Phys D Appl Phys*, 2015; **48:**22.
39. Replin Y, Proust C, Husson E, Beny JM. *J. Solid State Chem.*, 1995; **118:**163.
40. White BW, Kermidas VG, *Spectrochim. Acta, Part A,* 1972; **28:**501.
41. White L, Koo Y, Yun Y, Sankar J. *J. Nanomater.*, 2013; 1-8.
42. Chen F, Zhou H, Yao B, Qin Z, Zhang Q. *Surf. Coat. Technol.*, 2007; **201:**4905-4908.
43. Tan L, Wang Q, Geng F, Xi X, Qiu J, Yang K. *T Nonferr Metal Soc.*, 2010; **20:**s648-s654.